

Tuning the orbital-lattice fluctuations in the mixed spin-dimer system $\text{Ba}_{3-x}\text{Sr}_x\text{Cr}_2\text{O}_8$

Alsu Gazizulina,^{1,*} Diana Lucia Quintero-Castro,^{2,3,†} Dirk Wulferding,^{4,5} Jeremie Teyssier,⁶ Karel Prokes,³ Fabiano Yokaichiya,³ and Andreas Schilling¹

¹Physik-Institut, Universität Zürich, 8057 Zürich, Switzerland


²Department of Mathematics and Physics, University of Stavanger, 4036 Stavanger, Norway

³Helmholtz Zentrum Berlin für Materialien und Energie, 14109 Berlin, Germany

⁴Institute for Condensed Matter Physics, TU Braunschweig, 38106 Braunschweig, Germany

⁵Laboratory for Emerging Nanometrology (LENA), TU Braunschweig, 38106 Braunschweig, Germany

⁶Department of Quantum Matter Physics, University of Geneva, 1211 Geneva, Switzerland

 (Received 11 July 2018; revised manuscript received 25 September 2018; published 31 October 2018)

In $\text{A}_3\text{Cr}_2\text{O}_8$, where $A = \text{Sr}$ or Ba , the Cr^{5+} ions surrounded by oxygen ions in a tetrahedral coordination are Jahn-Teller active. The Jahn-Teller distortion leads to a structural transition and a related emergence of three twinned monoclinic domains below the structural phase transition. This transition is highly *dynamic* over an extended temperature range for $A = \text{Sr}$. We have investigated mixed compounds $\text{Ba}_{3-x}\text{Sr}_x\text{Cr}_2\text{O}_8$ with $x = 2.9$ and $x = 2.8$ by means of x-ray and neutron diffraction, Raman scattering, and calorimetry. Based on the obtained evolution of the phonon frequencies, we find a distinct suppression of the orbital-lattice fluctuation regime with increasing Ba content. This stands in contrast to the linear behavior exhibited by unit cell volumes, atomic positions, and intradimer spin-spin exchange interactions.

DOI: [10.1103/PhysRevB.98.144115](https://doi.org/10.1103/PhysRevB.98.144115)

I. INTRODUCTION

In many condensed matter systems, e.g. manganites, ferrites, cuprates, among others, the key to functional magnetoelectronic properties is the interaction between degenerate orbital degrees of freedom and lattice fluctuations through a cooperative Jahn-Teller effect [1–6]. This effect can eventually change the crystallographic structure, fully lift the orbital degeneracy, or create a short-range orbital order through a dynamical Jahn-Teller distortion. Spin-spin correlations are also relevant in these strongly correlated compounds and can interact with orbital and lattice degrees of freedom. Even more, interesting dynamics can emerge when the spin-spin correlations are spatially frustrated, leading to a macroscopic degeneracy of the ground state [7].

All these competing degrees of freedom are present in $\text{A}_3\text{Cr}_2\text{O}_8$ (with $A = \text{Ba}, \text{Sr}$). These systems consist of a three-dimensional network of coupled spin dimers formed by Cr^{5+} . The single $3d$ electron of the chromium ion has a twofold orbital degeneracy, which makes the system Jahn-Teller active. The dimers are antiferromagnetically linked in a triangular in-plane arrangement, resulting in a certain degree of magnetic frustration. A Jahn-Teller transition is reported at temperatures $T_{JT} = 285$ K for $\text{Sr}_3\text{Cr}_2\text{O}_8$ [8] and $T_{JT} = 70$ K for $\text{Ba}_3\text{Cr}_2\text{O}_8$ [9]. The Jahn Teller transition is related to a structural transition from trigonal $R\bar{3}m$ to monoclinic $C2/c$ appearing in both compounds (Fig. 1) [10]. The magnetic frustration is lifted thanks to this structural distortion creating three twin domains and leading to

spatially anisotropic exchange interactions [11,12]. The main characteristic parameters for these systems are listed in Table I.

Raman scattering investigations performed on a single crystal of $\text{Sr}_3\text{Cr}_2\text{O}_8$ have found that new phonons, linked to the $C2/c$ space group, are not emerging right below the Jahn-Teller transition, but instead there is an extended temperature regime where the lattice is fluctuating [13]. This lattice fluctuation regime was linked to orbital ordering and further changes in the orbital sector below the Jahn-Teller transition temperature T_{JT} [8]. These fluctuations are reduced with decreasing temperature and all the modes of the monoclinic structure are observed when the temperature is lower than T^* . This is not the case for $\text{Ba}_3\text{Cr}_2\text{O}_8$ where there is no sign of orbital fluctuations below T_{JT} [9].

Multiple parameters contribute to the heat capacity in this compound, the orbital gap between the $d_{3z^2-r^2}$ and $d_{x^2-y^2}$, the spin gap, the lattice contribution, and the Jahn-Teller transition anomaly. Analysis of the heat capacity in $\text{Sr}_3\text{Cr}_2\text{O}_8$ [8], together with ESR data [14], allowed us to extract an orbital gap of 388 K and a spin gap of 27 K. On the other hand, measurements of the heat capacity in $\text{Ba}_3\text{Cr}_2\text{O}_8$ have allowed us to determine corresponding entropy which reaches a value slightly lower than expected [9]. An important difference between these compounds is that $\text{Ba}_3\text{Cr}_2\text{O}_8$ recovers all the orbital entropy after the Jahn Teller transition, whereas $\text{Sr}_3\text{Cr}_2\text{O}_8$ exceeds that entropy reaching a value slightly higher than expected [8]. Measurements of the orbital gap in $\text{Ba}_3\text{Cr}_2\text{O}_8$ have not been reported.

The differences in the dynamic lattice-orbital properties between these two systems stand in contrast to their magnetic ground state (singlet) and magnetic excitations (triplons) which are essentially similar in both compounds [11,12,14].

*alsu@physik.uzh.ch

†diana.l.quintero@uis.no

TABLE I. Table of the parameters for $\text{Sr}_3\text{Cr}_2\text{O}_8$ and $\text{Ba}_3\text{Cr}_2\text{O}_8$ taken from literature [9,11–13]. J_0 and J_e are intradimer and interdimer magnetic exchange interactions, respectively. T_{JT} is the Jahn-Teller transition temperature. T^* is the characteristic temperature, below which monoclinic structure modes are observed. Thus, $|T_{JT} - T^*|$ is the regime with strong fluctuations. V_c is the unit cell volume and $d_{\text{Cr-Cr}}$ is the closest distance of Cr-Cr ions that form the dimer.

	$\text{Sr}_3\text{Cr}_2\text{O}_8$	$\text{Ba}_3\text{Cr}_2\text{O}_8$
J_0 (K)	64	27
J_e/J_0	0.64	0.815
T_{JT} (K)	285	70
T^* (K)	156	70 ($= T_{JT}$)
$ T_{JT} - T^* $ (K)	119	0
V_c (\AA^3)	541.7	611.3
$d_{\text{Cr-Cr}}$ (\AA)	4.326	4.567

Intradimer (J_0) and interdimer (J_e) magnetic exchange interactions for both compounds are listed in Table I.

It is known that by mixing different cations in the atomic structure of functional materials, weak disorder can be introduced and it may be sufficient to change physical properties dramatically [4,15]. Many exotic phases can be observed in mixed condensed matter electronic systems, such as perovskites [16] and cuprates [5], where unusual strong orbit-lattice coupling has been observed [17]. The abundance of functional properties in those mixed systems is stimulated by a static displacive disorder due to differences in ionic radii, which creates mixed charge distribution [18]. However, the complex magnetic phase diagrams by settling of very different long range magnetic order as a function of cation mixing present in many of these compounds make the direct study of the orbital dynamics nontrivial.

Recently, we reported on the effect of chemical substitution on the magnetic properties of $\text{Ba}_{3-x}\text{Sr}_x\text{Cr}_2\text{O}_8$ upon partially replacing Sr by Ba by 3.3% and 6.6%. It was found that the intradimer spin-spin interaction is smaller in the mixed compound with $x = 2.9$ than in pure $\text{Sr}_3\text{Cr}_2\text{O}_8$ by 4%, whereas the interdimer exchange interactions are reduced by 7% [19]. No sign of magnetic disorder was found. Furthermore, we

have found that the critical magnetic field related to the condensation of the triplet magnetic excitations decreases monotonically with x [20]. This change is in accordance with the change of the intradimer interaction constant J_0 [21].

Here, we report on the study of the *dynamic* structural phase distortions in the mixed systems $\text{Ba}_{3-x}\text{Sr}_x\text{Cr}_2\text{O}_8$ (with $x = 2.8, 2.9$). Both pristine and mixed compounds preserve the magnetic ground state and are therefore the ideal model systems to study uniquely orbit-lattice fluctuations as a function of cation mixing. We investigated the structural phase transition in the mixed compounds over an extended temperature range. Using heat capacity measurements, Raman scattering, neutron single crystal diffraction, and high-resolution x-ray powder diffraction techniques, we have explored the variation of the crystal structure of $\text{Ba}_{3-x}\text{Sr}_x\text{Cr}_2\text{O}_8$ (with $x = 2.9$ and $x = 2.8$) as a function of temperature.

II. EXPERIMENTAL DETAILS

Single crystals of $\text{Ba}_{3-x}\text{Sr}_x\text{Cr}_2\text{O}_8$ were grown with $x = 2.9$ and $x = 2.8$, as described in Ref. [19]. Heat capacity measurements were performed in a physical property measurement system (PPMS, Quantum Design Inc.).

The temperature dependent high-resolution powder x-ray diffraction experiments were carried out at the Swiss-Norwegian beamline BM01 at the ESRF in Grenoble [22]. Temperature control was achieved using a liquid nitrogen cryostream. A powder sample of $\text{Ba}_{0.1}\text{Sr}_{2.9}\text{Cr}_2\text{O}_8$ was measured in the temperature range from 100 K to 300 K. To extract crystallographic lattice parameters and atomic displacement positions, Rietveld refinement was performed using the FullProf software [23].

The nuclear structure of the spin dimer system $\text{Ba}_{3-x}\text{Sr}_x\text{Cr}_2\text{O}_8$ with $x = 2.9$ was studied by performing single crystal neutron diffraction on the two-axis-diffractometer E4 at the Helmholtz Zentrum für Materialien und Energie in Berlin. The sample with a volume $\cong 1 \text{ cm}^3$ was mounted with $(h, h, l)_h$ in the scattering plane (subindices h and m correspond to hexagonal and monoclinic notation, respectively). The incident wavelength was 2.4 \AA . Measurements of intensities of key Bragg peaks were made at temperatures between 1.5 K and 290 K.

Raman scattering experiments were performed using an excitation wavelength of $\lambda = 514.5 \text{ nm}$ on single crystals of $\text{Ba}_{3-x}\text{Sr}_x\text{Cr}_2\text{O}_8$ with $x = 2.9$ and $x = 2.8$. Samples were embedded in a silver matrix to achieve better thermalization. Both crystals were mounted and polished parallel to the ac plane. The incoming laser polarization was along the c axis and scattered light of all polarizations was detected. The laser power was set to 0.5 mW with a spot diameter of about $2 \mu\text{m}$. Scans were recorded in 10 K steps from 5 K up to 200 K, followed by 20 K steps in the range 200 K to 340 K.

III. RESULTS AND DISCUSSION

In the mixed compounds $\text{Ba}_{3-x}\text{Sr}_x\text{Cr}_2\text{O}_8$, the magnetic ion Cr^{5+} is surrounded by four oxygen ions in a tetrahedral symmetry, as shown in Fig. 2(a). A cooperative Jahn-Teller distortion lifts the electronic degeneracy of tetrahedrally coordinated Cr^{5+} ions. At $T > T_{JT}$, the structure is hexagonal

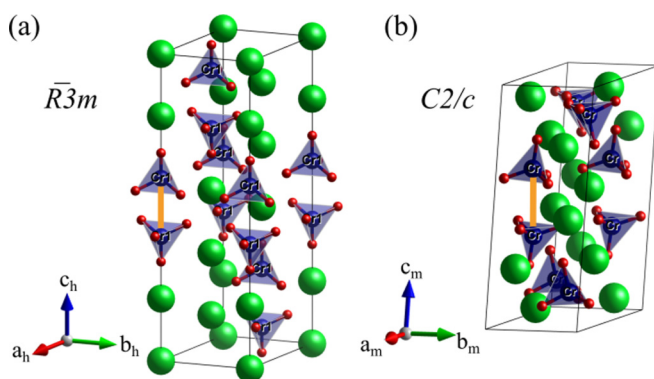


FIG. 1. (a) Hexagonal and (b) monoclinic unit cells in $\text{A}_3\text{Cr}_2\text{O}_8$. Cr^{5+} ions, represented in blue, are located in oxygen tetrahedra, O^{2-} ions are represented by red spheres, and $A = \text{Sr/Ba}$ by green spheres. Dimer bonds are represented in orange.

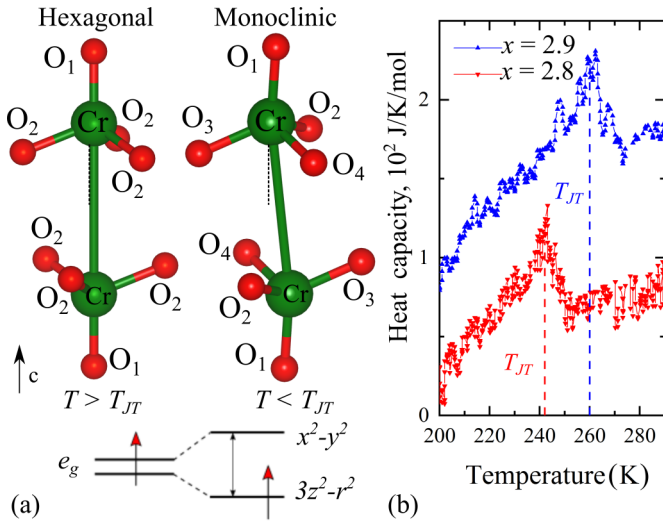


FIG. 2. (a) Two CrO_4 tetrahedra forming a dimer unit in the hexagonal and the monoclinic phases (top). Corresponding occupation of electronic levels in each phase (bottom). (b) Heat capacity-temperature dependences for both samples: $x = 2.9$ (black curve) and $x = 2.8$ (red curve) showing λ -like Jahn-Teller transitions at 260 K and 242 K, respectively.

in the space group $R\bar{3}m$. Bilayers of CrO_4 tetrahedra form a frustrated arrangement of two degenerate $3d^1 e_g$ levels ($3z^2 - r^2$ and $x^2 - y^2$). Each orbital is coupled to the displacement of the O atoms surrounding the ion. For $T < T_{JT}$, crystallographic distortions lead to the monoclinic structure $C2/c$ and a splitting of the levels of the lower-lying orbitals. This structural transition is characterized by an antiferrodistortive displacement of the apical O_1 oxygen ions and a slight rotation of the O_2 ions in the tetrahedral bottom plane within each dimer. It leads to three twinned monoclinic domains in the parent compounds $\text{Sr}_3\text{Cr}_2\text{O}_8$ [11] and $\text{Ba}_3\text{Cr}_2\text{O}_8$ [12].

Recently, we showed that introducing Ba in the $\text{Sr}_3\text{Cr}_2\text{O}_8$ system does lead neither to magnetic disorder nor to intragap intensities in the dispersion relation [19]. The Jahn-Teller distortion temperature in $\text{Ba}_{3-x}\text{Sr}_x\text{Cr}_2\text{O}_8$ is gradually suppressed with decreasing x , as shown in Ref. [24], and vanishes for intermediate stoichiometries x . This transition is reflected as a λ -like transition in the heat capacity, as measured for $x = 2.9$ and $x = 2.8$ [Fig. 2(b)]. For the mixed compounds $x = 2.9$ and $x = 2.8$, the Jahn-Teller transition temperatures are $T_{JT} = 260$ K and 242 K, whereas for the pure $\text{Sr}_3\text{Cr}_2\text{O}_8$ T_{JT} is 285 K and 70 K for $\text{Ba}_3\text{Cr}_2\text{O}_8$, respectively [12,13].

In the x-ray powder diffraction patterns, obtained at temperatures above T_{JT} for $x = 2.9$ compound, the observed Bragg reflections were indexed using the space group $R\bar{3}m$. Our analysis of those patterns shows that the lattice at $T < T_{JT}$ is then better described using the space group $C2/c$, however, with new diffraction peaks gradually appearing as can be seen in Fig. 3(a). Our results are in agreement with density functional theory calculations of the orbital ordering in $\text{Sr}_3\text{Cr}_2\text{O}_8$ that demonstrate the strong electron correlation which arises within the $3d^1$ shell and can clearly explain a phase transition leading to the stabilization of its

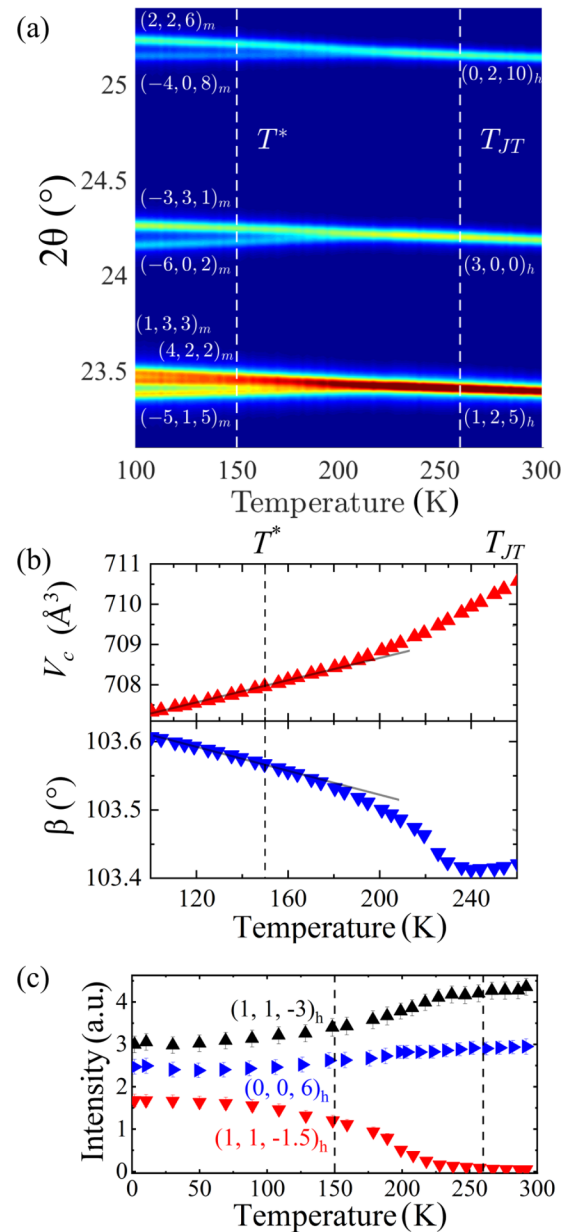


FIG. 3. (a) Color contour plot of the temperature dependence of the x-ray diffraction pattern for $x = 2.9$ powder. The centered reflection $(3, 0, 0)_h$ splits into $(-6, 0, 2)_m$ and $(-3, 3, 1)_m$ at lower temperatures. (b) Temperature dependence of the integrated intensity of $(1,1,-3)_h$, $(1,1,-1.5)_h$, and $(0, 0, 6)_h$ reflections of a $x = 2.9$ single crystal. Dotted lines show $T_{JT} = 260$ K and $T^* = 150$ K. (c) The unit cell volume and monoclinic angle β in the monoclinic symmetry $C2/c$ as a function of temperature (red and blue data points, respectively). The lines are guides to the eye.

monoclinic $C2/c$ space-group symmetry and spin-singlet magnetic ground state [25].

The crystallographic parameters extracted by using Rietveld refinement [23] are presented in Table II. The weighted profile R factor shows a relatively good fit. The lattice parameters and unit cell volume shrink in a nonlinear manner as a function of temperature [Fig. 3(b)]. Apart from the unit cell volume and lattice constants, the structural distortion

TABLE II. Crystallographic parameters extracted from the Rietveld refinement of the BM01 data for $x = 2.9$. The weighted profile R factor is $R_{wp} \cong 8$ for both refinements, at $T < T^*$ (100 K) and at $T > T_{JT}$ (300 K).

$x = 2.9$	$C2/c$ (100 K)		$R\bar{3}m$ (300 K)	
a (Å)	9.60(8)		5.57(7)	
b (Å)	5.51(6)		5.57(7)	
c (Å)	13.72(7)		20.20(6)	
α (deg)	90		90	
β (deg)	$\cong 103.61(3)$		90	
γ (deg)	90		120	
Atom	Atomic position (x, y, z) _{<i>m</i>}	$B_{iso\ m}$ (Å ²)	Atomic position (x, y, z) _{<i>h</i>}	$B_{iso\ h}$ (Å ²)
Cr	(0.2028, 0.2557, 0.8576)	0.84(7)	(0, 0, 0.4052)	0.79(9)
Sr ₁ /Ba ₁	(0, 0.2715, 0.2500)	0.46(1)	(0, 0, 0)	0.79(9)
Sr ₂ /Ba ₂	(0.1020, 0.2482, 0.5550)	0.42(8)	(0, 0, 0.2037)	0.64(9)
O ₁	(0.1602, 0.3086, 0.7386)	0.38(5)	(0, 0, 0.3255)	0.97(8)
O ₂	(0.1143, 0.7842, 0.5987)	0.85(6)	(0.8353, 0.1647, 0.8981)	0.97(8)
O ₃	(0.8624, -0.0091, 0.6078)	0.42(4)		
O ₄	(0.3683, 0.9842, 0.5833)	0.61(2)		

also affects the monoclinic angle β . The monoclinic angle decreases nonlinearly by $\Delta\beta \approx 0.12^\circ$ when increasing the temperature from 80 K to 220 K, as can be seen in Fig. 3(b), and deviates slightly from the value that is expected from a conversion between the rhombohedral and the monoclinic space groups [21].

Previously, Chapon *et al.* reported a neutron diffraction study on Sr₃Cr₂O₈. Several superlattice reflections were observed well below T_{JT} , which can be indexed by a propagation vector $k = (0, 0, 3/2)$ within the space group $C2/c$. Interpretation of the Bragg peak intensities requires a large anisotropic displacement parameter on the oxygen site O₁. This displacement increases on cooling. The tetrahedral distortion changes the crystal field of the sample, therefore it affects directly Jahn Teller energies and the splitting of orbitals. The distortion of the CrO₄ can be described by the tetrahedral angles, namely O₁-Cr-O₃ (α_{1-3}) and O₁-Cr-O₄ (α_{1-4}). For Sr₃Cr₂O₈ ($x = 3$) $\alpha_{1-3} = 117.2^\circ$ and $\alpha_{1-4} = 104.5^\circ$, whereas for $x = 2.9$, we found $\alpha_{1-3} = 114.56^\circ$ and $\alpha_{1-4} = 108.02^\circ$. However, a crystallographic study of Ba₃Cr₂O₈ has not been reported.

The structural distortion is characterized by an antiferrodistortive displacement of the apical O₁ oxygen ion within the CrO₄ tetrahedra similar to Sr₃Cr₂O₈ [10]. The displacement of O₁ is coupled to the displacement of the Sr₁/Ba₁ and a slight rotation of the tetrahedral basal plane, spanned by the O₂ ions. This rotation and distortion further modifies the Cr-O distances below T_{JT} to O₂, O₃, and O₄. A modification of the Cr-O distances leads to a change in energy of the electronic orbitals of Cr⁵⁺. The crystalline electric field splits the 3d orbitals of the Cr⁵⁺ ion into lower-lying nonbonding e_g orbitals and higher-lying antibonding t_{2g} orbitals. This distortion reduces the point group symmetry of the Cr⁵⁺ site from C_{3v} (in Schoenflies notation) in the hexagonal structure to C_1 in the monoclinic structure where the e_g state degeneracy is lifted, with a separation into $(3z^2 - r^2)$ and $(x^2 - y^2)$ orbitals. The oxygen tetrahedron around the Cr⁵⁺ ion is only slightly affected by varying the temperature and changes only with the onset of the structural transition at T_{JT} .

Single crystal neutron diffraction was also performed in order to obtain detailed information about the formation

of three monoclinic twins by measuring key reflections in the $(h, h, l)_h$ plane, which correspond to a unique, double, or triple twin, as a function of temperature. The results are shown in Fig. 3(c). Three reflections were measured: $(1, 1, -3)_h$, $(1, 1, -1.5)_h$, and $(0, 0, 6)_h$. The reflection $(1, 1, -1.5)_h$ corresponds to two different monoclinic reflections $(1, 1, -1.5)_h = (0, 2, 1)_{m^{(1,2)}} = (3, 1, 2)_{m^{(3)}}$, where the $m^{(n)}$ notation corresponds to the n th monoclinic twin. The reflection $(0, 0, 6)_h$ corresponds to three monoclinic twins $(0, 0, 6)_h = (0, 0, 4)_{m^{(1,2,3)}}$ and it is an allowed hexagonal reflection, and the $(1, 1, -3)_h$ reflection is allowed in both hexagonal and monoclinic and corresponds to the reflections $(1, 1, -3)_h = (0, 2, 2)_{m^{(1)}} = (3, 1, 3)_{m^{(2,3)}}$. Conversions from hexagonal to monoclinic Miller indices have been done following Ref. [11]. The monoclinic unit cell relates to the hexagonal cell by the transformation $a_{m1} = a_h - b_h$, $b_{m1} = a_h + b_h$, $c_{m1} = a_h/3 - b_h/3 + 2c_h/3$, $a_{m2} = 2a_h + b_h$, $b_{m2} = b_h$, $c_{m2} = 2a_h/3 + b_h/3 + 2c_h/3$, $a_{m3} = a_h + 2b_h$, $b_{m3} = -a_h$, $c_{m3} = a_h/3 + 2b_h/3 + 2c_h/3$.

The largest changes of the diffraction patterns are observed for temperatures far below the Jahn-Teller transition temperature T_{JT} reaching full intensities well below T_{JT} . The observed dependences indicate that the structure stabilizes below some characteristic temperature $T^* < T_{JT}$, which we define more precisely further below.

Figure 4(a) shows two Raman spectra collected at 320 K and 10 K. At low temperatures two modes develop between 310 and 340 cm⁻¹. They are rather broad as compared to other peaks. This indicates a possible mixing of the orbital excitation and a phonon. A factor group analysis [13] gives the number of Raman active phonons that was analyzed for the parent compound Sr₃Cr₂O₈. 11 Raman active phonon modes are expected in the hexagonal symmetry $R\bar{3}m$ and 39 corresponding modes in the monoclinic space group $C2/c$ out of which only 26 modes were observed. The respective mode frequencies and their symmetry assignments are given in Ref. [13]. We detected only slight shifts in the phonon frequencies when compared with the parent compound Sr₃Cr₂O₈.

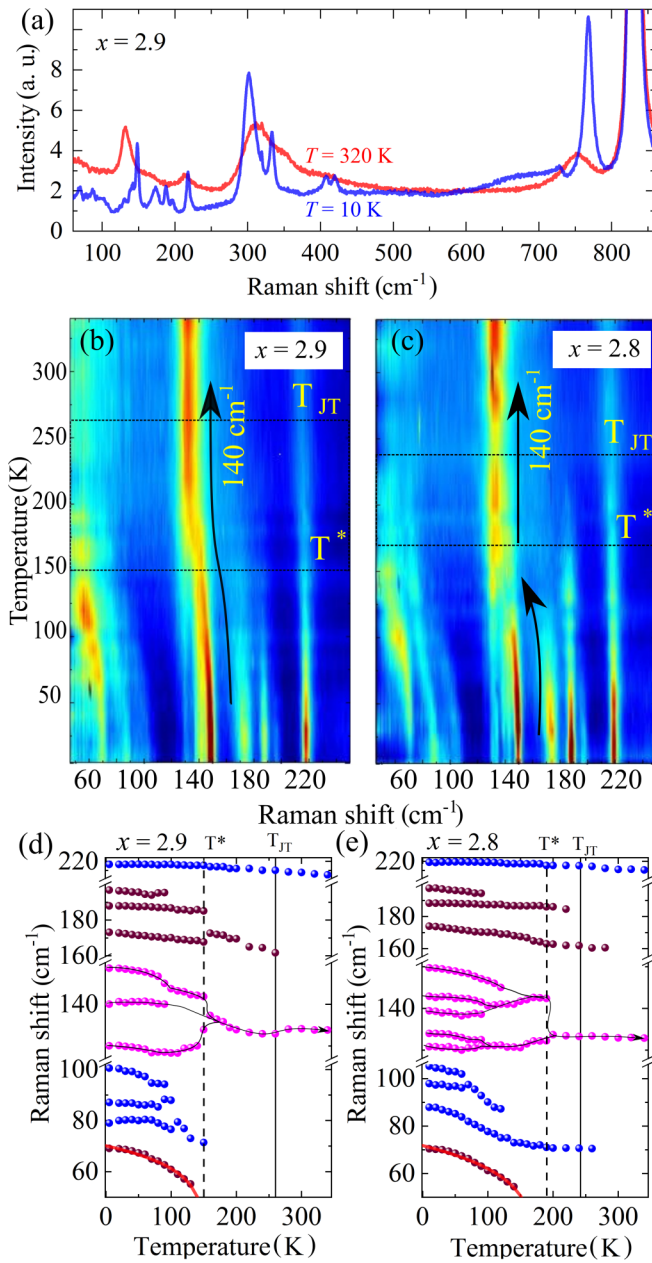


FIG. 4. (a) Raman spectra collected at $T = 320$ K (red curve) and at 10 K (blue curve) for $x = 2.9$. Color plot spectra in the temperature range from 5 K to 340 K for (b) $x = 2.9$ and (c) $x = 2.8$. Temperature evolution of the phonon frequencies for (d) $x = 2.9$ and (e) $x = 2.8$. The red line is a fit of the mode around 70 cm^{-1} .

We observe distinct changes in the phonon spectra in the temperature range 100–260 K [see Figs. 4(b) and 4(c)]. Below a temperature around 150 K ($= T^*$) for $x = 2.9$, the quasielastic scattering (seen as a subtle increase in scattering intensity towards low energies) is suppressed and the Raman spectra show a behavior that can be described as a stabilization of the lattice. Therefore, T^* marks a crossover from orbital fluctuations to long-range and static structural distortions and we can therefore interpret the temperature window between T^* and T_{JT} as a range with strong fluctuations. The strong electron correlation arising within the $3d$ shell of Cr^{5+} can

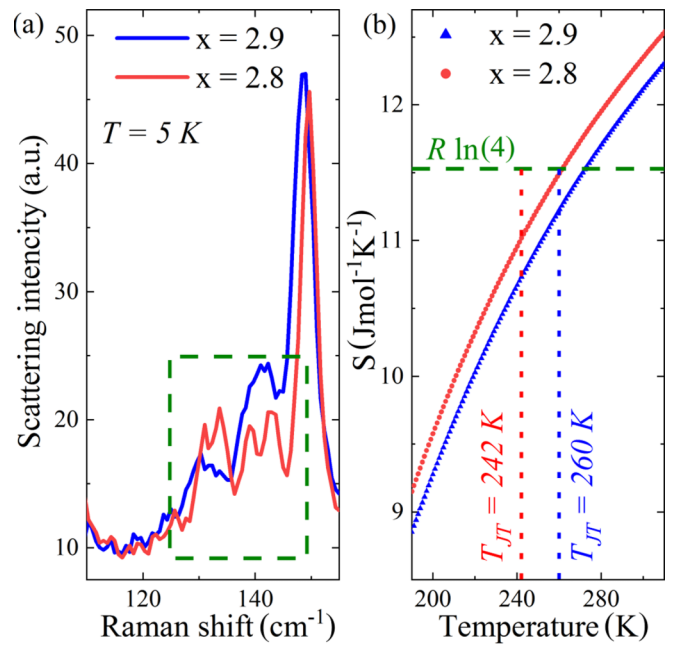


FIG. 5. (a) Scattering intensity of Raman spectra collected at $T = 5$ K for $x = 2.9$ (blue curve) and $x = 2.8$ (red curve). Puncture green box shows the range of Raman shift from 110 cm^{-1} to 150 cm^{-1} . (b) Temperature evolution of the entropy S calculated from the heat capacity data [Fig. 2(b)] for $x = 2.9$ (blue curve) and $x = 2.8$ (red curve). The green puncture line is the entropy limit $S = R \ln 4$.

explain the phase transition leading to the stabilization of the monoclinic $C2/c$ space group symmetry.

Following the analysis for $\text{Sr}_3\text{Cr}_2\text{O}_8$ [13], the lattice degrees of freedom are very dynamic and they share a common characteristic energy scale with the orbital degrees of freedom (i.e., the orbital gap energy). This was taken as evidence that there is a strong coupling between them. Considering that the overall behavior of the $x = 2.9$ and the $x = 2.8$ compounds is not dissimilar to the $x = 3$ compound, we would not expect some fundamentally different mechanisms as a source for fluctuations in these systems.

Taking a closer look at the phonon mode around 140 cm^{-1} , the transition is very smooth between 200 K and 150 K in the case of $x = 2.9$, whereas for $x = 2.8$ there seems to be a more pronounced jump around 125 K [see marks in Figs. 4(b) and 4(c)].

Moreover, two more modes at 139 and 136 cm^{-1} emerge for $x = 2.8$ in contrast with $x = 2.9$ at temperatures below T^* . Figure 5(a) shows the scattering intensity or Raman spectra at $T = 5$ K for both compounds: $x = 2.9$ and $x = 2.8$. We assume that the observed splitting exists for the $x = 2.9$ compound as well but within the resolution limit of our experiment was not clearly observed. Indeed, the asymmetric phonon lineshapes for the $x = 2.9$ sample suggest a superposition of multiple modes. The entropy associated with the orbital degrees of freedom can be evaluated from the heat capacity data. Figure 5(b) shows the entropy for $x = 2.9$ and $x = 2.8$. Entropy reaches $R \ln(4)$ and is the sum of the orbital and magnetic contributions, where R is the molar gas constant [9]. Since there is essentially one spin dimer per unit

of formula $A_3Cr_2O_8$, the magnetic contribution to the entropy should be $2R \ln(2)$. On the other hand, the e orbitals of each Cr^{5+} ion are degenerate, and the orbital degrees of freedom will contribute to the entropy of another $2R \ln(2)$, where two Cr^{5+} ions per unit of formula are taken into account. Comparable to $x = 3$, corresponding entropy reaches a value slightly higher than the expected $R \ln(4)$.

We can conclude that there is a slightly different fluctuating behavior for the lattice of two compounds. In Figs. 4(d) and 4(e), the frequencies of the phonon modes, extracted with a Lorentz fitting, are plotted as a function of temperature. Both samples, $x = 2.9$ and $x = 2.8$, show similar trends in their temperature evolution with a strong softening of the $3A_g$ modes at about 70, 90, and 105 cm^{-1} . In particular, the mode around 70 cm^{-1} evidences a dramatic softening upon increasing the temperature towards T^* due to a strong coupling to electronic degrees of freedom. This mode is very susceptible to the atomic displacement of the apical oxygen O_1 in the CrO_4 tetrahedra, and the related displacement may correspond to a possible rotational motion of the CrO_4 tetrahedra that modifies all Cr-O distances. This mode behaves like an order parameter when going from the phase with degenerate energy levels into the distorted phase with the Jahn-Teller-split energy levels. Consequently, the mode is strongly related to the orbital ordering. Therefore, once the Jahn-Teller distortion changes the transition from dynamic to static at T^* , this soft mode starts to emerge. This process can be viewed as a static tetrahedral distortion. Thus, we can consider this phonon energy as a secondary order parameter, that emerges from orbital order and can be described by mean-field theory, $\omega(T) = A |T^* - T|^\eta$ [see fits in Figs. 4(d) and 4(e)], where η denotes the critical exponent of the secondary order parameter and T^* indicates the critical temperature of the transition [26]. We obtain $\eta = 0.12$ and 0.16 for $x = 2.9$ and $x = 2.8$, respectively. These exponents are close to the two-dimensional Ising solution where $\eta = 1/8$. A similar mean-field exponent has been extracted from a soft phonon mode in the related Jahn-Teller active $BaNi_2Fe[VO_4]_2$ [27].

Based on the mean-field fit to the soft mode energy 70 cm^{-1} , we obtain $T^* = (150 \pm 3)$ K for $x = 2.9$ and $T^* = (170 \pm 5)$ K for $x = 2.8$. Interestingly, T^* for $x = 2.8$ is noticeably enhanced in comparison with $x = 2.9$. This means that the fluctuation regime is narrowed with increasing Ba content and fluctuations are suppressed. Figure 6 shows the temperature range of the fluctuation regime $|T_{JT} - T^*|$ and the intradimer magnetic exchange interaction J_0 as a function of Sr content x in $Ba_{3-x}Sr_xCr_2O_8$. Values for the end members $Ba_3Cr_2O_8$ and $Sr_3Cr_2O_8$ are taken from literature [9,13]. The interaction J_0 changes monotonously in the shown region of x but not linearly as the lattice parameters [21]. The area below the data points of the temperature range $|T_{JT} - T^*|$ marked by yellow color is a guide for the eye. It shows that the fluctuation regime decreases drastically and would vanish around $x = 2.72$.

There are different plausible scenarios leading to a decrease in T_{JT} and a suppression of the fluctuation regime upon increasing Ba content: One possibility could be disorder or bond length mixing induced by Ba/Sr substitution. However, our experiments evidence a systematic trend, where the end members (with the lowest level of disorder) mark the two ex-

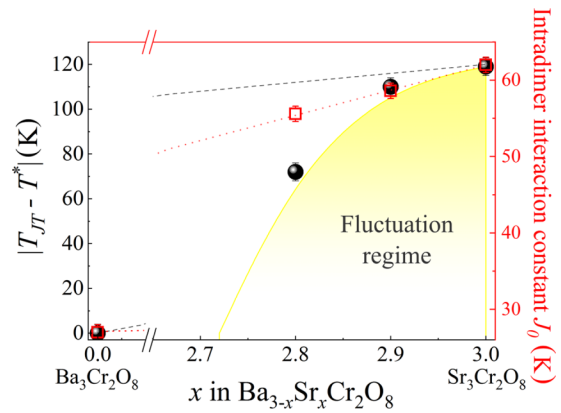


FIG. 6. Temperature range of the fluctuation regime $|T_{JT} - T^*|$ (filled black spheres) and intradimer interaction J_0 (open red squares, Ref. [19]) versus Sr content x in $Ba_{3-x}Sr_xCr_2O_8$. Lines in the respective color indicate a linear dependence of these quantities on the Sr content x for comparison.

trema cases of no fluctuations vs maximum fluctuations. Since lattice constants and unit cell volume change linearly [21] as a function of x , there is also no obvious structural reason for the suppression of T^* . A more likely scenario is a continuous tuning of the intradimer interaction J_0 (shown on the right axis of Fig. 6) as well as the ratio of inter- to intradimer interaction J'/J_0 with x . In fact it was found that for $Ba_3Cr_2O_8$ this ratio is slightly larger ($J'/J_0 = 0.82$) than for $Sr_3Cr_2O_8$ ($J'/J_0 = 0.64$) [19]. This subtle difference could be the reason for the fundamentally different dynamics. An observed stronger interdimer coupling J' (with respect to J_0) can lead to a faster stabilization of the spin- and the orbital subsystem, whereas a weaker interdimer coupling preserves a low-dimensional quantum magnetism character of the spin dimer system, which is more prone to strong fluctuations.

Lattice dynamics can be present in the hexagonal lattice in order to achieve a thermodynamically favored orbitally nondegenerate ground state of a Jahn-Teller active ion in a distorted environment. Similar to $Ba_{3-x}Sr_xCr_2O_8$, a dynamical transition has been observed in different materials, such as $BaNi_2Fe[VO_4]_2$ where the transition is induced by the gradual evolution of the distortion around FeO_6 [27]. Another example of dynamical orbital correlation is the spin state transition in $LaCoO_3$ where the state changes gradually due to short-range orbital order [4]. A strong suppression of the Jahn-Teller-type crystal field with the lowering of structural symmetry was found in oxides such as $LaVO_3$ upon cooling [28]. Moreover, $KCuF_3$, a material with Kugel-Khomskii-type orbital order and similar to high- T_c superconducting cuprate perovskites, exhibits a large temperature range of structural fluctuations starting at the high-temperature structural transition, and extending down to the lower structural transition, which corresponds to a freezing of the octahedral rotations [6].

IV. CONCLUSIONS

Our heat capacity, Raman scattering, neutron, and x-ray diffraction experiments reveal an extended orbit-lattice fluctuation regime.

tuation regime that is narrowed upon Ba substitution. Orbital ordering with suppressed orbital fluctuations is found to be reached far below the structural Jahn-Teller transition T_{JT} in $x = 2.9$ and $x = 2.8$. Our investigations demonstrate the stabilization of the monoclinic $C2/c$ space-group symmetry below a characteristic temperature T^* in $\text{Ba}_{3-x}\text{Sr}_x\text{Cr}_2\text{O}_8$. The Raman spectra change drastically with decreasing temperatures and the coherent part of lattice distortions develops only at lower temperatures. Complete crystallographic studies of these series of samples will be performed in the future.

The *dynamic* structural phase distortion discussed here is caused by strong orbital fluctuations. We have discussed different scenarios leading to a decrease in T_{JT} and the suppression of the fluctuation regime upon increasing Ba content. We conclude that a strong interdimer magnetic exchange interaction in the spin dimer network could support the fast stabilization of the orbit-lattice state, whereas large values of J_0 lead to individual decoupled dimers, making the system more susceptible to fluctuations. Therefore, small modifica-

tions in the three-dimensional magnetic exchange interactions could be of more crucial importance to stabilize different structural/orbital states in spin-charge-orbital couple systems, e.g., cuprates, manganites, ferrites, etc., than small changes in unit cell volumes or atomic positions.

ACKNOWLEDGMENTS

We thank B. Lake for the access to the crystal growth laboratory, A. T. M. Nazmul Islam for the technical assistance, and the Helmholtz Zentrum Berlin for the access to neutron beam time at the research reactor BER II. We thank D. Chernyshov for the discussion and measurements at Swiss-Norwegian beamline BM01 at the ESRF in Grenoble. We thank G. Thorkildsen and O. Zavorotynska for useful discussion. A.G. is supported by the Swiss National Science Foundation Grant No. 21-153659 and SCOPES IZ747Z0_160527. D.W. acknowledges financial support from the Quantum- and Nano-Metrology (QUANOMET) initiative within project NL-4.

-
- [1] J. Varignon, N. C. Bristowe, E. Bousquet, and P. Ghosez, *Sci. Rep.* **5**, 15364 (2015).
- [2] A. Stroppa, P. Barone, P. Jain, J. M. Perez-Mato, and S. Picozzi, *Adv. Mater.* **25**, 2284 (2013).
- [3] A. Kyono, S. A. Gramsch, Y. Nakamoto, M. Sakata, M. Kato, T. Tamura, and T. Yamanaka, *Am. Mineral.* **100**, 1752 (2015).
- [4] Y. Tokura and N. Nagaosa, *Science* **288**, 5465 (2000).
- [5] H. Keller, A. Bussmann-Holder, and K. A. Müller, *Mater. Today* **11**, 38 (2008).
- [6] J. C. T. Lee, S. Yuan, S. Lal, Y. Il Joe, Y. Gan, S. Smadici, K. Finkelstein, Y. Feng, A. Rusydi, P. M. Goldbart, S. L. Cooper, and P. Abbamonte, *Nat. Phys.* **8**, 63 (2012).
- [7] S. Pal and S. Lal, *Phys. Rev. B* **96**, 075139 (2017).
- [8] Z. Wang, M. Schmidt, A. Günther, S. Schaile, N. Pascher, F. Mayr, Y. Goncharov, D. L. Quintero-Castro, A. T. M. N. Islam, B. Lake, H.-A. Krug von Nidda, A. Loidl, and J. Deisenhofer, *Phys. Rev. B* **83**, 201102(R) (2011).
- [9] Z. Wang, M. Schmidt, A. Günther, F. Mayr, Y. Wan, S.-H. Lee, H. Ueda, Y. Ueda, A. Loidl, and J. Deisenhofer, *Phys. Rev. B* **85**, 224304 (2012).
- [10] L. C. Chapon, C. Stock, P. G. Radaelli, and C. Martin, *arXiv:0807.0877*.
- [11] D. L. Quintero-Castro, B. Lake, E. M. Wheeler, A. T. M. N. Islam, T. Guidi, K. C. Rule, Z. Izaola, M. Russina, K. Kiefer, Y. Skourski, and T. Herrmannsdorfer, *Phys. Rev. B* **81**, 014415 (2010).
- [12] M. Kofu, H. Ueda, H. Nojiri, Y. Oshima, T. Zenmoto, K. C. Rule, S. Gerischer, B. Lake, C. D. Batista, Y. Ueda, and S.-H. Lee, *Phys. Rev. Lett.* **102**, 177204 (2009).
- [13] D. Wulferding, P. Lemmens, K.-Y. Choi, V. Gnezdilov, Y. G. Pashkevich, J. Deisenhofer, D. Quintero-Castro, A. T. M. Nazmul Islam, and B. Lake, *Phys. Rev. B* **84**, 064419 (2011).
- [14] Z. Wang, D. Kamenskyi, O. Cépas, M. Schmidt, D. L. Quintero-Castro, A. T. M. N. Islam, B. Lake, A. A. Aczel, H. A. Dabkowska, A. B. Dabkowski, G. M. Luke, Y. Wan, A. Loidl, M. Ozerov, J. Wosnitza, S. A. Zvyagin, and J. Deisenhofer, *Phys. Rev. B* **89**, 174406 (2014).
- [15] A. Zheludev and T. Roscilde, *C. R. Phys.* **14**, 740 (2013).
- [16] R. Maezono, S. Ishihara, and N. Nagaosa, *Phys. Rev. B* **58**, 11583 (1998).
- [17] J.-Q. Yan, J.-S. Zhou, and J. B. Goodenough, *Phys. Rev. Lett.* **93**, 235901 (2004).
- [18] E. Dagotto, *Science* **309**, 257 (2005).
- [19] A. Gazizulina, D. L. Quintero-Castro, and A. Schilling, *Phys. Rev. B* **96**, 184201 (2017).
- [20] H. Grundmann, A. Sabitova, A. Schilling, F. von Rohr, T. Forster, and L. Peters, *New J. Phys.* **18**, 033001 (2016).
- [21] H. Grundmann, A. Schilling, C. A. Marjerrison, H. A. Dabkowska, and B. D. Gaulin, *Mater. Res. Bull.* **48**, 3108 (2013).
- [22] V. Dyadkin, Ph. Pattison, V. Dmitriev, and D. Chernyshov, *Synchrotron Rad.* **23**, 825 (2016).
- [23] J. Rodriguez-Carvajal, *Physica B (Amsterdam)* **192**, 55 (1993).
- [24] H. Grundmann, A. Schilling, M. Medarde, and D. Sheptyakov, *Phys. Rev. B* **90**, 075101 (2014).
- [25] G. Radtke, A. Saul, H. A. Dabkowska, G. M. Luke, and G. A. Botton, *Phys. Rev. Lett.* **105**, 036401 (2010).
- [26] L. D. Landau and E. M. Lifshitz, *Statistical Physics*, Third Edition, Vol. 5 (Butterworth-Heinemann, Imprint, 1980).
- [27] A. Reuß, V. Ksenofontov, J. Tapp, D. Wulferding, P. Lemmens, M. Panthöfer, and A. Möller, *Inorg. Chem.* **57**, 6300 (2018).
- [28] M. Kim and B. I. Min, *Phys. Rev. B* **89**, 121106(R) (2014).